

HVS-Based Model for Superposition of Two Color Halftones

Altyngul Jumabayeva; School of Electrical and Computer Engineering, Purdue University, West Lafayette, IN 47907, U.S.A.;

Tal Frank; Hewlett-Packard Indigo Division, Rehovot, Israel;

Yotam Ben-Shoshan; Hewlett-Packard Indigo Division, Rehovot, Israel;

Robert Ulichney; Hewlett-Packard Laboratories USA, Cambridge, MA 02142, U.S.A.;

Jan Allebach; School of Electrical and Computer Engineering, Purdue University, West Lafayette, IN 47907, U.S.A.

Abstract

In this paper, we look into the superposition of two periodic clustered-dot color halftones, which are widely used for electrophotographic printers due to their print stability. The scope of our research lies in understanding how to make the best color assignments to the two regular or irregular halftones in order to minimize the perceived error. We develop a model that agrees with a human observer and allows fast implementation. In order to account for the difference in the responses of the human viewer to luminance and chrominance information, we use the $Y_y C_x C_z$ color space, which is a linearized version of the $L^*a^*b^*$ uniform color space. The perceived error helps us identify the configuration of colors and screens that will improve the appearance of the superposition image. We believe that making the right color assignments is essential for developing high quality color images.

Introduction

The purpose of our research¹ is to design a predictor that will help us assign colorants to different screens that will minimize the perceived error. In addition, we would like to find out what are the advantages and disadvantages in using regular and irregular halftones for the superposition. In our previous work, which was based on a single separation, we made a conclusion that choosing an irregular halftone screen has an advantage of getting closer to the target screen tile vector. However, it results in higher graininess levels. Whereas with a regular screen, the distance from the target screen tile vector is increased, but the graininess levels may improve [4]. Another challenge that we are facing is that as we explore the superposition of two irregular color halftones, we need not only take into account the effects of superposition but also the effects of digitization. In order to eliminate dot-on-dot printing in the superposition image, the screen of each colorant is rotated to a different angle. However, this causes other problems such as moire and rosette artifacts, which are the result of the interaction between two lattices. The moire phenomenon refers to a low-frequency structure, which has a very visible pattern and can be observed at the superposition of two halftones, and not in the individual halftones separately [3]. In contrast, a rosette pattern has a circular or polygonal pattern, which is formed as a result of rotating halftone screens [3]. The superposition of two color halftones is a very important question to study because the artifacts such as moire, rosette and misregistration can lead to color shifts. Baqai and Allebach presented a systematic method for designing moire- and rosette- free clustered-dot color screens for

discrete raster color systems [3]. Whereas Ufuk and Allebach developed a model-based color halftoning method which minimizes the perceived error between the continuous tone original color image and the color halftone image [2]. In our research, we integrate the HVS based model that takes into account the spectral representation of color and the difference in the responses of the human viewer to luminance and chrominance information in order to obtain the perceived error metrics. Specifically, we are interested in investigating the new challenges that occur as a result of superimposing the two irregular halftone screens in comparison to the two regular halftone screens.

Method

The procedure implemented in our research consists of three parts. The first part involves generating the three $g_X[\mathbf{m}]$, $g_Y[\mathbf{m}]$, and $g_Z[\mathbf{m}]$ images of the superposition halftone. In the second part, in order to account for the difference in the responses of the human viewer to luminance and chrominance information, we use a linearized version of the $L^*a^*b^*$ uniform color space, which is $Y_y C_x C_z$ [1]. And lastly, in part three we apply separate luminance and chrominance frequency responses; and we obtain the average squared perceived error.

Color device model

We start by considering the superposition of two colorants. The halftone patterns of the cyan and magenta colorants associated with their periodicity matrices \mathbf{N}_c and \mathbf{N}_m are represented as $g_c[\mathbf{m}]$ and $g_m[\mathbf{m}]$ in Fig. 1. The superposition of these two halftones generates three colorant areas (Neugebauer primaries) c , m , cm , and a white w area. In order to transform to a device-independent space CIE XYZ, we use the Neugebauer primaries generator to obtain a $g_{NP}[\mathbf{m}]$ image. Next, we obtain the XYZ

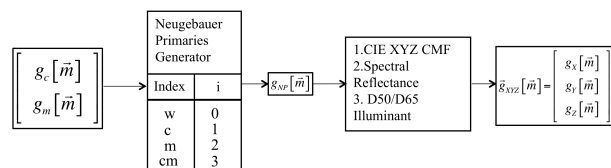


Figure 1. The procedure for generating images in CIE XYZ.

matrix using the spectral reflectance, the CIE XYZ color matching functions (CMF's), and a D65 Illuminant, depicted in Figs. 2, 3, and 4. X , Y , and Z values are obtained using the following

¹Research supported by the Hewlett-Packard Company, Palo Alto, CA.

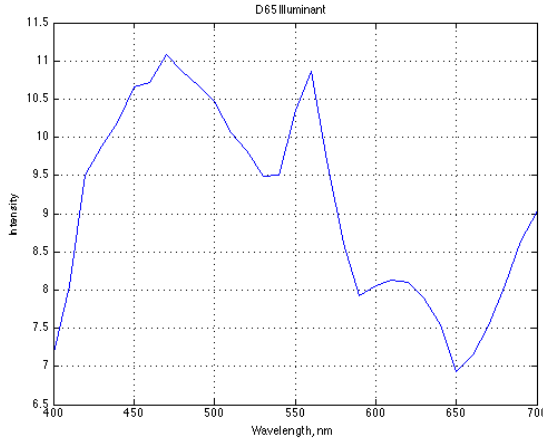


Figure 2. D65 Illuminant.

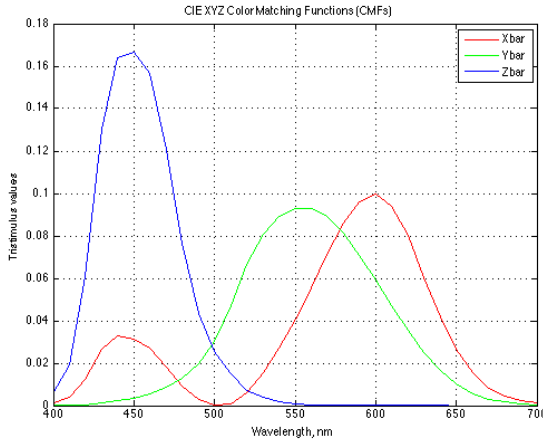


Figure 3. CIE XYZ Color Matching Functions.

equations:

$$\begin{aligned} X &= \int_{400}^{700} S(\lambda)\bar{x}(\lambda)d\lambda \\ Y &= \int_{400}^{700} S(\lambda)\bar{y}(\lambda)d\lambda \\ Z &= \int_{400}^{700} S(\lambda)\bar{z}(\lambda)d\lambda, \end{aligned} \quad (1)$$

where

$$S(\lambda) = I(\lambda)R(\lambda). \quad (2)$$

Here, we define $I(\lambda)$ to be the Illuminant function, for example D50 Illuminant or D65 Illuminant, and $R(\lambda)$ to be the Reflectance function corresponding to the specific Neugebauer primary, including the media on which the colorant is placed. It is unique to the target printer. In this paper, we use the Ideal Block Reflectance functions, shown in Fig. 4 for the cyan and magenta colorants only, and the D65 Illuminant to illustrate our results.

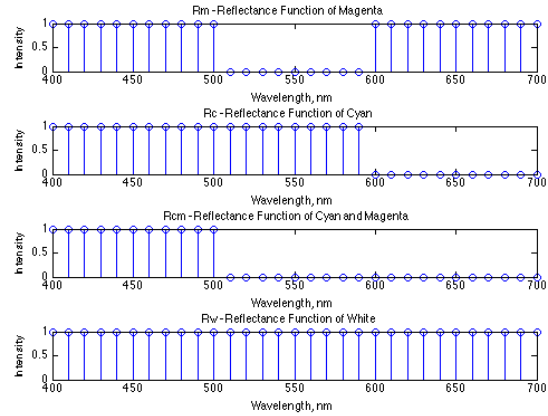


Figure 4. Ideal Block Reflectance for cyan and magenta colorants.

The final XYZ matrix has the following form:

$$XYZ = \begin{bmatrix} X_c & X_m & X_{cm} & X_w \\ Y_c & Y_m & Y_{cm} & Y_w \\ Z_c & Z_m & Z_{cm} & Z_w \end{bmatrix}. \quad (3)$$

Lastly, to get the $g_X[\mathbf{m}]$, we use the previously obtained $g_{NP}[\mathbf{m}]$ and the X values for c, m, cm , and w :

$$g_X[\mathbf{m}] = \begin{cases} X_w, & g_{NP}[\mathbf{m}] = 0 \\ X_c, & g_{NP}[\mathbf{m}] = 1 \\ X_m, & g_{NP}[\mathbf{m}] = 2 \\ X_{cm}, & g_{NP}[\mathbf{m}] = 3. \end{cases} \quad (4)$$

The $g_Y[\mathbf{m}]$ and $g_Z[\mathbf{m}]$ images are similarly obtained.

Opponent color space

Next, we implement the human visual model that accounts for the difference in the responses of the human viewer to luminance and chrominance information. We use a linearized version of $L^*a^*b^*$ color space in order to preserve local averages, which are crucial for faithful tone reproduction [1]. The transformation that we use is:

$$\begin{aligned} Y_y &= 116 \frac{Y}{Y_n} \\ C_x &= 500 \left[\frac{X}{X_n} - \frac{Y}{Y_n} \right] \\ C_z &= 200 \left[\frac{Y}{Y_n} - \frac{Z}{Z_n} \right], \end{aligned} \quad (5)$$

where (X_n, Y_n, Z_n) is the D65 white point for the XYZ color space. The Y_y component represents luminance, and C_x and C_z components represent the $R - G$ and $B - Y$ opponent-color chrominance components. In order to look at each channel separately, we convert each channel to sRGB by setting the other two channels to 0 or a constant value [1]. For example, in order to look at the Y_y channel, we set C_x , and C_z channels to 0 resulting in $(Y_y, 0, 0)$. After that we transform back to XYZ and to sRGB [1]. Figure 5 summarizes the procedure. It turned out after the transformation

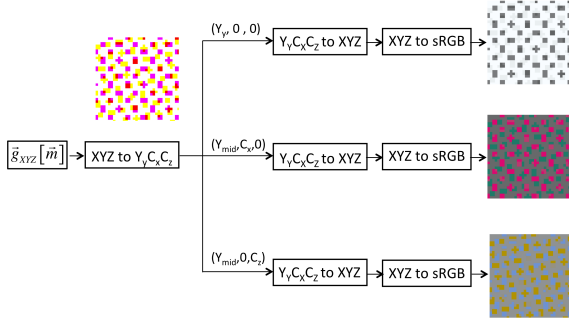


Figure 5. Visualization of Y_y , C_x and C_z channels in sRGB. Y_{mid} is the midpoint between the maximum and the minimum values in the Y_y component

of $(Y_{mid}, C_x, 0)$ and $(Y_{mid}, 0, C_z)$ from XYZ to sRGB, there were negative values in sRGB at some pixels. In order to not lose any data, we developed a procedure, that will fit all the data inside the range $[0, 1]$. Figure 6 depicts the procedure for visualizing $(Y_{mid}, 0, C_z)$. A similar approach is used to display $(Y_{mid}, C_x, 0)$. In addition to Fig. 6, a detailed derivation for obtaining the α parameter is provided in the Appendix.

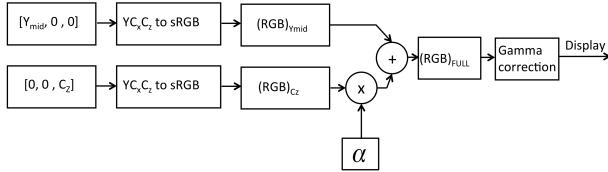


Figure 6. Procedure for visualizing $(Y_{mid}, 0, C_z)$.

Spatial Frequency Response and Error Metrics

The next step is to apply separate luminance and chrominance frequency responses to Y_y , C_x and C_z , which are chosen based on the spatial sensitivity of the human eye to them. For the luminance channel, we use Daly HVS, which is given as:

$$H(\bar{\rho}) = \begin{cases} a(b + c\bar{\rho}) \exp(-c\bar{\rho}^d), & \bar{\rho} > \bar{\rho}_{max} \\ 1, & \text{else,} \end{cases} \quad (6)$$

where $a = 2.2, b = 0.192, c = 0.114, d = 1.1, \bar{\rho}_{max} = 6.6$, and $\bar{\rho} = \sqrt{u^2 + v^2}$ [5]. For the chrominance channel, we use the approximation by Kolpatzik and Bouman to experimental data collected by Mullen, which is given as:

$$W(\bar{\rho}) = A \exp(-\alpha \|\bar{\rho}\|), \quad (7)$$

where $\alpha = 0.419$, and $A = 100$ [1], [3]. The procedure is demonstrated in Fig. 7. After obtaining $\epsilon_{Y_y}(i, j)$, $\epsilon_{C_x}(i, j)$, $\epsilon_{C_z}(i, j)$ for each pixel of the image located at (i, j) , and scaling $\epsilon_{Y_y}(i, j)$ by 4, we calculate $\Delta E(i, j)$ in the following way:

$$\Delta E(i, j) = \sqrt{(\epsilon_{Y_y}(i, j)^2 + \epsilon_{C_x}(i, j)^2 + \epsilon_{C_z}(i, j)^2)}. \quad (8)$$

Finally, we obtain the $\Delta E_{average}$ value, using:

$$\Delta E_{average} = \frac{1}{mn} \sum_{i=1}^m \sum_{j=1}^n \Delta E(i, j), \quad (9)$$

where the size of the image is $m \times n$. Knowing $\Delta E_{average}$ helps us identify which color should be assigned to which screen in order to decrease the graininess of the superposition image.

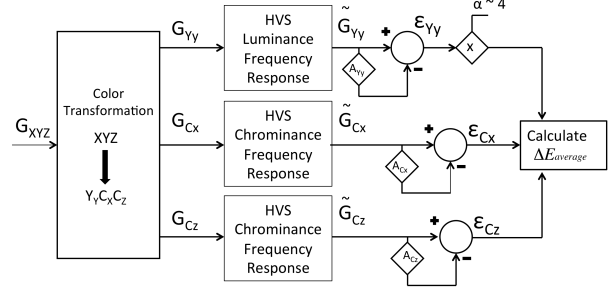


Figure 7. The procedure for obtaining the main components for calculating $\Delta E_{average}$. $\tilde{G}_{Y_y}(\mathbf{u})$, $\tilde{G}_{C_x}(\mathbf{u})$, and $\tilde{G}_{C_z}(\mathbf{u})$ represent the perceived Fourier Transforms of their corresponding images $\tilde{g}_{Y_y}[\mathbf{m}]$, $\tilde{g}_{C_x}[\mathbf{m}]$, and $\tilde{g}_{C_z}[\mathbf{m}]$.

Results

Since the scope of our research lies in investigating the behavior of irregular clustered dot halftones, we chose to work with two irregular halftone screens and 3 colorants: cyan, magenta, and yellow. The first screen is an irregular screen with a periodicity matrix $N_1 = \begin{bmatrix} 9/2 & -1 \\ 1 & 9/2 \end{bmatrix}$, and the second screen is also an

irregular screen with a periodicity matrix $N_2 = \begin{bmatrix} 10/3 & -10/3 \\ 10/3 & 10/3 \end{bmatrix}$.

For the HP Indigo press with resolution 812.8 dpi, these screens have frequencies 176.32 and 172.42 lpi, respectively. Their angles are 12.53 and 45 degrees, respectively. Since we have 2 halftone screens and 3 colorants, we need to compare 6 different sets of data, defined and indexed in Table 1. Based on Table 1, with Su-

Table 1. 6 configurations for 2 halftone screens and 3 colorants: cyan, magenta, and yellow

Index (#)	$N_1 = \begin{bmatrix} 9/2 & -1 \\ 1 & 9/2 \end{bmatrix}$	$N_2 = \begin{bmatrix} 10/3 & -10/3 \\ 10/3 & 10/3 \end{bmatrix}$
1	Cyan	Magenta
2	Magenta	Cyan
3	Yellow	Magenta
4	Magenta	Yellow
5	Cyan	Yellow
6	Yellow	Cyan

perposition #1 the halftone with periodicity matrix N_1 is cyan, and the halftone with periodicity matrix N_2 is magenta. It is presented in Fig. 9. Figure 10 reveals the visualization of the opponent channels in sRGB. In order to get a better insight of the opponent color channels, the zoomed-in view of Y_y , C_x , and C_z is provided in Fig. 8. The $Y_y C_x C_z$ matrix corresponding to the XYZ matrix mentioned in Equation 3 has the following form:

$$\begin{bmatrix} Y_y \\ C_x \\ C_z \end{bmatrix} = \begin{bmatrix} 101.51 & 33.03 & 11.75 & 122.80 \\ -124.05 & 140.59 & 44.21 & -27.67 \\ -50.96 & -145.85 & -177.08 & -19.73 \end{bmatrix} \quad (10)$$

Similar to Equation 3, columns 1 through 4 correspond to the cyan, magenta, cyan and magenta, and white pixels in the superposition image. From Fig. 8, it can be seen that the magenta pixel, which is the sum of red and blue, has a large red component in the C_x channel with its corresponding value of 140.59 and a large blue component in the C_z image with its corresponding value of -145.85 based on Equation 10. Whereas the cyan pixel, which is the sum of green and blue, has a large green component in the C_x channel with its value of -124.05, but a much smaller blue component in the C_z channel with its value of -50.96. Figure 11 is a visualization of the opponent color channels filtered with their corresponding luminance and chrominance frequency responses depicted in the Methods section. The filtered $(Y_y, 0, 0)$ image has a strongly visible low frequency pattern, whereas the filtered C_x , and C_z images have no visible pattern due to the nature of the chrominance filter. As a comparison to the Superposition #1 results, the detailed results for the Superposition #2, when the halftone with periodicity matrix N_2 is cyan, and the halftone with periodicity matrix N_1 is magenta, are presented in Figs. 12, 13, and 14. Based on Fig. 14, it can be deduced that the filtered $(Y_y, 0, 0)$ image has a less visible low frequency pattern than the $(Y_y, 0, 0)$ image of Superposition #1, which is also verified by the calculated $\Delta E_{average}$ values, which are provided in Table 2, and supported by their corresponding images in Fig. 15. Our results emphasize that in the case of Ideal Block Reflectance and D65 Illuminant, we get a higher $\Delta E_{average}$ when applying the magenta colorant to a more irregular screen if choosing between either magenta and yellow, or magenta and cyan configurations. In this paper, the more irregular screen is $N_2 = \begin{bmatrix} 10/3 & -10/3 \\ 10/3 & 10/3 \end{bmatrix}$. That's why the $\Delta E_{average}$ for configurations #1 and #3 is higher than their complementary pairs. Similarly, $\Delta E_{average}$ is higher for configuration #6, when the cyan colorant is applied to a more irregular halftone rather than the yellow colorant. The results may seem intuitive for these simple cases. However, when considering different sets of regular and irregular screens, and different sets of Illuminants and Spectral Reflectance Functions, the results may no longer be easily predicted.

Conclusion

We have presented the HVS-based model for the superposition of two clustered dot color halftones, which assists us in

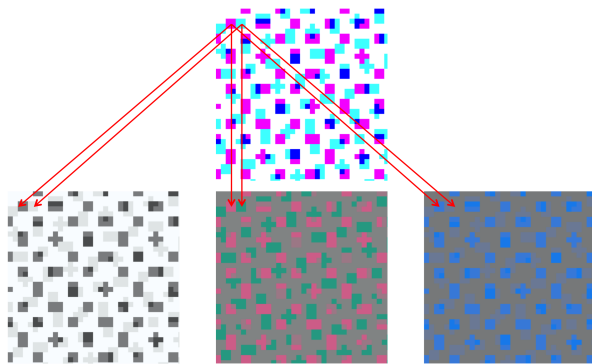


Figure 8. Zoomed-in view of Y_y , C_x , and C_z channels for the Superposition #1.

making the right choices when assigning colorants to a variety of irregular or regular screens. We used the $Y_y C_x C_z$ color space in order to account for the difference in the responses of the human viewer to luminance and chrominance information. Our model can be used to improve the predictions concerning the visibility of color halftone textures. Next, we plan to study and learn more about the superposition of three and four clustered dot color halftones.

Appendix

Our goal is to display an image defined as $(Y_{mid}, 0, C_z)$ in sRGB space, which we specify as

$$RGB_{FULL} = (R_{C_z}^{FULL}, G_{C_z}^{FULL}, B_{C_z}^{FULL}). \quad (11)$$

However, when we convert directly, we have negative values in sRGB space, which correspond to the opponency of channels (Y, C_x, C_z) . We use the fact that

$$(Y_{mid}, 0, C_z) = (Y_{mid}, 0, 0) + (0, 0, C_z). \quad (12)$$

After converting an image $(Y_{mid}, 0, 0)$ from XYZ space to sRGB space, we obtain the image $(R_{Y_{mid}}, G_{Y_{mid}}, B_{Y_{mid}})$. Similarly, converting an image $(0, 0, C_z)$ from XYZ space to sRGB space, we obtain the image $(R_{C_z}, G_{C_z}, B_{C_z})$.

Therefore,

$$(R_{C_z}^{FULL}, G_{C_z}^{FULL}, B_{C_z}^{FULL}) = \Delta(R_{C_z}, G_{C_z}, B_{C_z}) + (R_{Y_{mid}}, G_{Y_{mid}}, B_{Y_{mid}}), \quad (13)$$

where

$$\begin{aligned} \Delta R_{C_z}(m, n) &= R_{C_z}(m, n) - R_{Y_{mid}} \\ \Delta G_{C_z}(m, n) &= G_{C_z}(m, n) - G_{Y_{mid}} \\ \Delta B_{C_z}(m, n) &= B_{C_z}(m, n) - B_{Y_{mid}} \end{aligned} \quad (14)$$

Since the range of RGB_{FULL} should be from 0 to 1 for each channel, we define the new parameter α such that

$$(\tilde{R}_{C_z}^{FULL}, \tilde{G}_{C_z}^{FULL}, \tilde{B}_{C_z}^{FULL}) = \alpha \Delta(R_{C_z}, G_{C_z}, B_{C_z}) + (R_{Y_{mid}}, G_{Y_{mid}}, B_{Y_{mid}}). \quad (15)$$

We scale $\Delta(R_{C_z}, G_{C_z}, B_{C_z})$ by α , such that

$$0 \leq \alpha(\Delta R_{C_z}, \Delta G_{C_z}, \Delta B_{C_z}) + (R_{Y_{mid}}, G_{Y_{mid}}, B_{Y_{mid}}) \leq 1. \quad (16)$$

Therefore, for each channel, we have:

$$\begin{aligned} R_{C_z}^{FULL}(m, n) &= \alpha_R \Delta R_{C_z}(m, n) + R_{Y_{mid}} \\ G_{C_z}^{FULL}(m, n) &= \alpha_G \Delta G_{C_z}(m, n) + G_{Y_{mid}} \\ B_{C_z}^{FULL}(m, n) &= \alpha_B \Delta B_{C_z}(m, n) + B_{Y_{mid}}, \end{aligned} \quad (17)$$

such that

$$\begin{aligned} 0 &\leq \alpha_R \Delta R_{C_z}(m, n) + R_{Y_{mid}} \leq 1 \\ 0 &\leq \alpha_G \Delta G_{C_z}(m, n) + G_{Y_{mid}} \leq 1 \\ 0 &\leq \alpha_B \Delta B_{C_z}(m, n) + B_{Y_{mid}} \leq 1, \end{aligned} \quad (18)$$

and

$$\alpha = \min(\alpha_R, \alpha_G, \alpha_B). \quad (19)$$

The following assumptions have been made:

$$\begin{aligned} 0 < R_{Ymid} < 1 \\ 0 < G_{Ymid} < 1 \\ 0 < B_{Ymid} < 1 \\ (\alpha_R, \alpha_G, \alpha_B) > 0. \end{aligned} \quad (20)$$

We start by looking at the red channel.

$$0 \leq \alpha_R \Delta R_{Cz}(m, n) + R_{Ymid} \leq 1. \quad (21)$$

Part 1. Given that

$$\alpha_R \Delta R_{Cz}(m) + R_{Ymid} \leq 1, \quad (22)$$

we have

$$\begin{cases} \alpha_R \leq \frac{1-R_{Ymid}}{\Delta R_{Cz}(m, n)}, & \text{if } \Delta R_{Cz}(m, n) > 0 \\ \alpha_R \geq \frac{1-R_{Ymid}}{\Delta R_{Cz}(m, n)}, & \text{if } \Delta R_{Cz}(m, n) < 0. \end{cases} \quad (23)$$

The second equation in the system is satisfied by assumptions stated in the beginning that

$$\begin{aligned} 0 < R_{Ymid} < 1 \\ \alpha_R > 0. \end{aligned}$$

Therefore,

$$\alpha_R \geq \frac{1-R_{Ymid}}{\Delta R_{Cz}(m, n)}, \quad \text{if } \Delta R_{Cz}(m, n) < 0, \quad (24)$$

is always true. As for the first equation, we have

$$\alpha_R^+ \leq \min_{(m, n)} \left\{ \frac{1-R_{Ymid}}{\Delta R_{Cz}(m, n)}, \quad \text{if } \Delta R_{Cz}(m, n) > 0 \right\}. \quad (25)$$

Part 2. Given that

$$\alpha_R \Delta R_{Cz}(m) + R_{Ymid} \geq 0, \quad (26)$$

$$(27)$$

we have

$$\begin{cases} \alpha_R \geq \frac{-R_{Ymid}}{\Delta R_{Cz}(m, n)}, & \text{if } \Delta R_{Cz}(m, n) > 0 \\ \alpha_R \leq \frac{-R_{Ymid}}{\Delta R_{Cz}(m, n)}, & \text{if } \Delta R_{Cz}(m, n) < 0. \end{cases} \quad (28)$$

The first equation in the system is satisfied by assumptions stated before that

$$\begin{aligned} 0 < R_{Ymid} < 1 \\ \alpha_R > 0. \end{aligned}$$

Therefore

$$\alpha_R \geq \frac{-R_{Ymid}}{\Delta R_{Cz}(m, n)}, \quad \text{if } \Delta R_{Cz}(m, n) > 0. \quad (29)$$

As for the second equation, we have

$$\alpha_R^- \leq \min_{(m, n)} \left\{ \frac{-R_{Ymid}}{\Delta R_{Cz}(m, n)}, \quad \text{if } \Delta R_{Cz}(m, n) < 0 \right\}. \quad (30)$$

And lastly,

$$\alpha_R = \min(\alpha_R^+, \alpha_R^-). \quad (31)$$

α_G and α_B can be obtained similarly as α_R . And all three will be used to find

$$\alpha = \min(\alpha_R, \alpha_G, \alpha_B). \quad (32)$$

References

- [1] Thomas J. Flohr; Bernd W. Kolpatzik; Raja Balasubramanian; David A. Carrara; Charles A. Bouman, et al. "Model-based color image quantization", Proc. SPIE 1913, Human Vision, Visual Processing, and Digital Display IV, 270 (September 8, 1993); doi:10.1117/12.152701;
- [2] Ayse U. Agar and Jan P. Allebach "Model-Based Color Halftoning Using Direct Binary Search", IEEE Trans. on Image Processing, Vol. 14, pp. 1945-1959, Dec. 2005.
- [3] Farhan A. Baqai and Jan P. Allebach "Computer-aided design of clustered-dot color screens based on a human visual system model," Proc. IEEE, vol.90, no.1, pp.104,122, (January 2002); doi: 10.1109/5.982409
- [4] Altyngul Jumabayeva; Yi-Ting Chen; Tal Frank; Robert Ulichney and Jan Allebach "Design of irregular screen sets that generate maximally smooth halftone patterns", Proc. SPIE 9395, Color Imaging XX: Displaying, Processing, Hardcopy, and Applications, 93950K (January 8, 2015); doi:10.1117/12.2083553;
- [5] Sang Ho Kim and Jan P. Allebach "Impact of HVS Models on Model-Based Halftoning," IEEE Trans. on Image Processing, Vol. 11, pp. 258-269, March 2002.

Authors Biographies

Altyngul Jumabayeva received her BS in Electrical Engineering from Purdue University (2014) and is currently studying for the MS in Electrical Engineering. Her primary area of research has been the image graininess for regular and irregular clustered-dot halftones and the color superposition between them.

Yotam Ben-Shoshan received his BS in Electrical and Computer Engineering (2009) and MS in Electro-optics Engineering (2013) from the Ben-Gurion University of Negev, Israel. His research is mainly in the field of image processing. He currently serves as an algorithm engineer in the HP Indigo halftoning group.

Tal Frank has joined Indigo division 4.5 years ago and now leads the halftoning team. Tal holds BS in Physics and Mathematics from Bar Ilan University and MS in Physics from the Weizmann institute.

Robert Ulichney is a Distinguished Technologist with HP Labs focusing on systems for high capacity data embedding, and structures for variable density 3D printing. He received a Ph.D. from MIT in Electrical Engineering and Computer Science. Before joining HP he was with Digital Equipment Corp for several years then with Compaq's Cambridge Research Lab where he led a number of research projects on image and video implementations for both hard copy and display products.

Jan P. Allebach is Hewlett-Packard Distinguished Professor of Electrical and Computer Engineering at Purdue University. Allebach is a Fellow of the IEEE, the National Academy of Inventors, the Society for Imaging Science and Technology (IS&T), and SPIE. He was named Electronic Imaging Scientist of the Year by IS&T and SPIE, and was named Honorary Member of IS&T, the highest award that IS&T bestows. He has received the IEEE Daniel E. Noble Award, and is a member of the National Academy of Engineering. He currently serves as an IEEE Signal Processing Society Distinguished Lecturer (2016-2017).

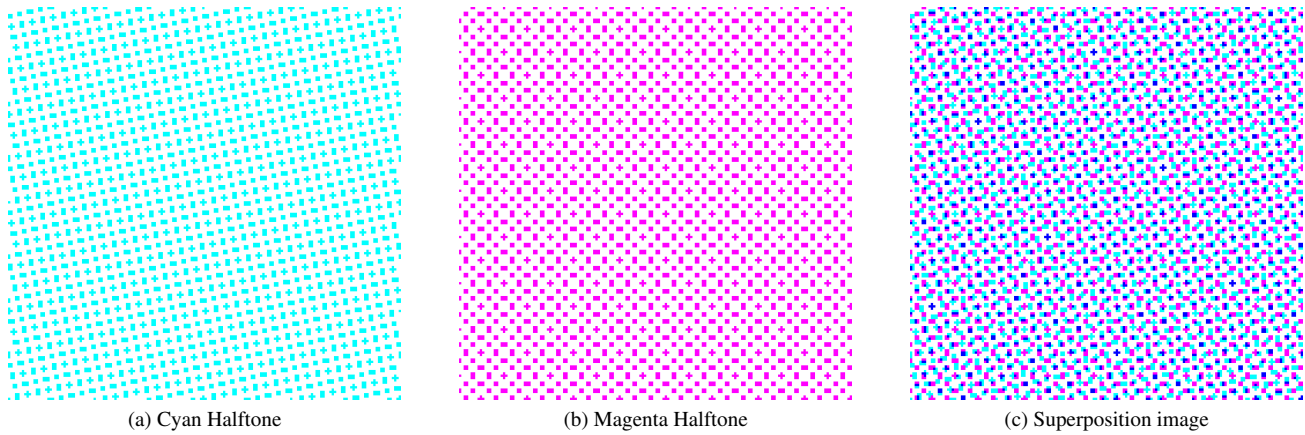


Figure 9. Superposition when the cyan halftone has a periodicity matrix N_1 and the magenta halftone has a periodicity matrix N_2

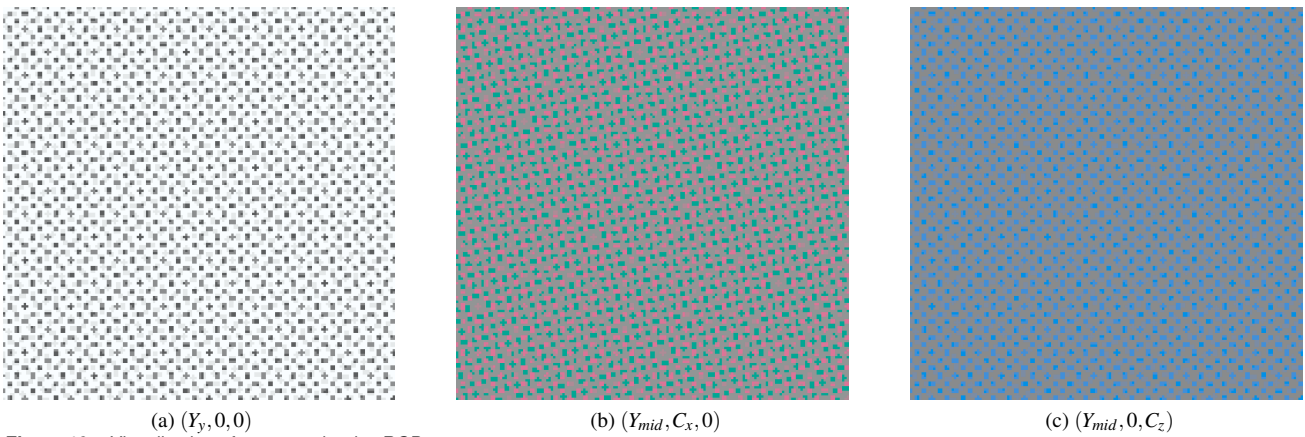


Figure 10. Visualization of Y_y , C_x , and C_z in sRGB.

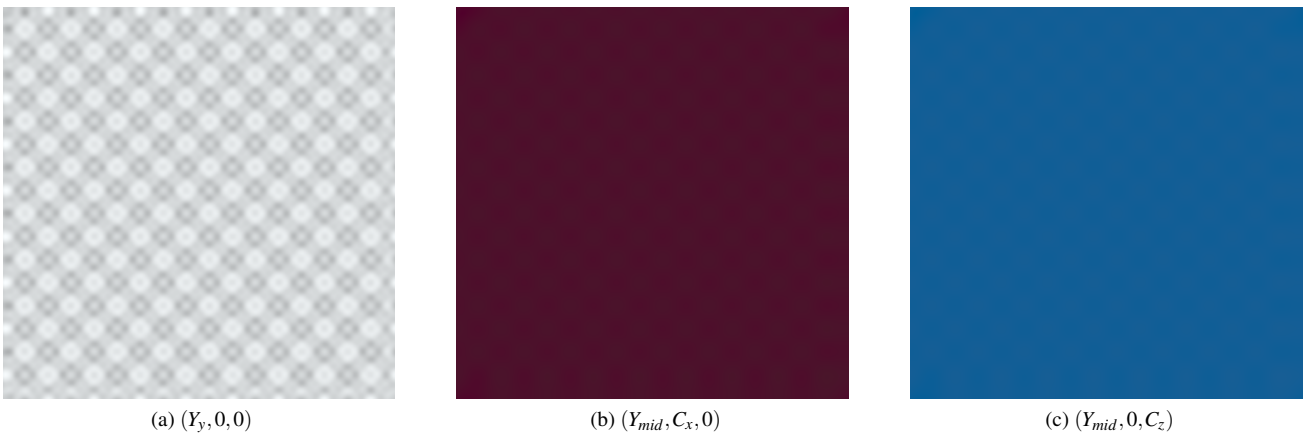


Figure 11. Visualization of Y_y , C_x , and C_z , filtered with luminance and chrominance frequency responses, in sRGB.

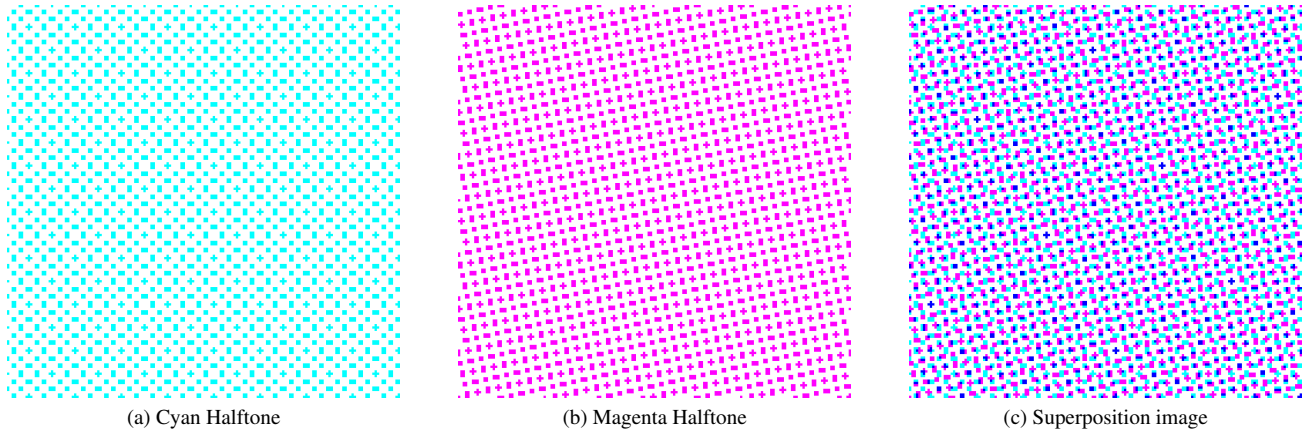


Figure 12. Superposition when the cyan halftone has a periodicity matrix N_2 and the magenta halftone has a periodicity matrix N_1

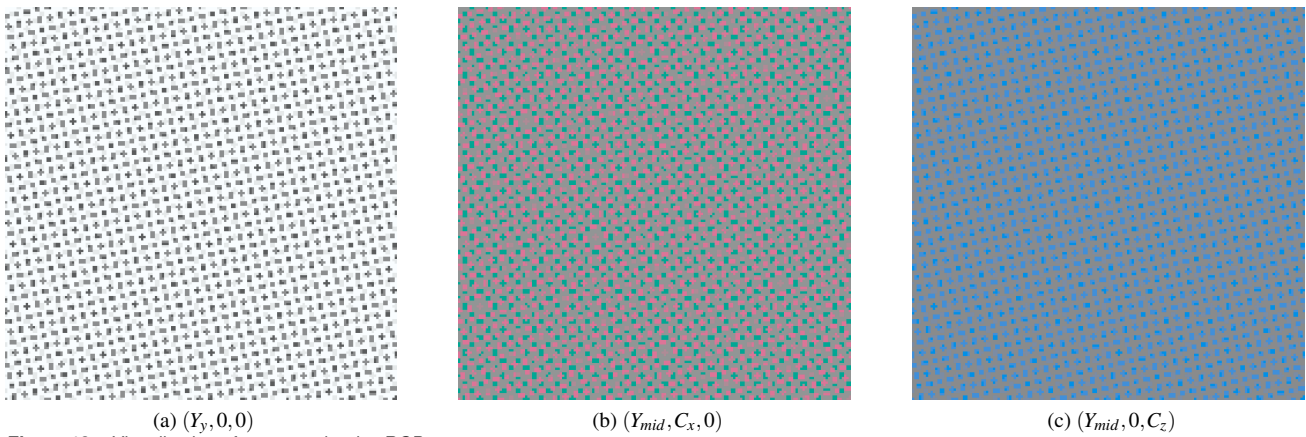


Figure 13. Visualization of Y_y , C_x , and C_z in sRGB.

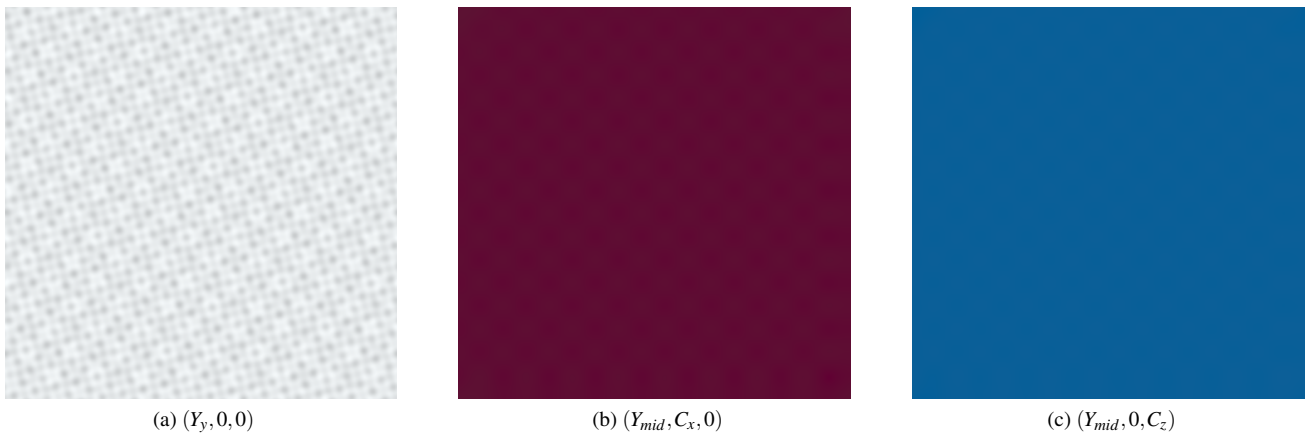


Figure 14. Visualization of Y_y , C_x , and C_z , filtered with luminance and chrominance frequency responses, in sRGB.

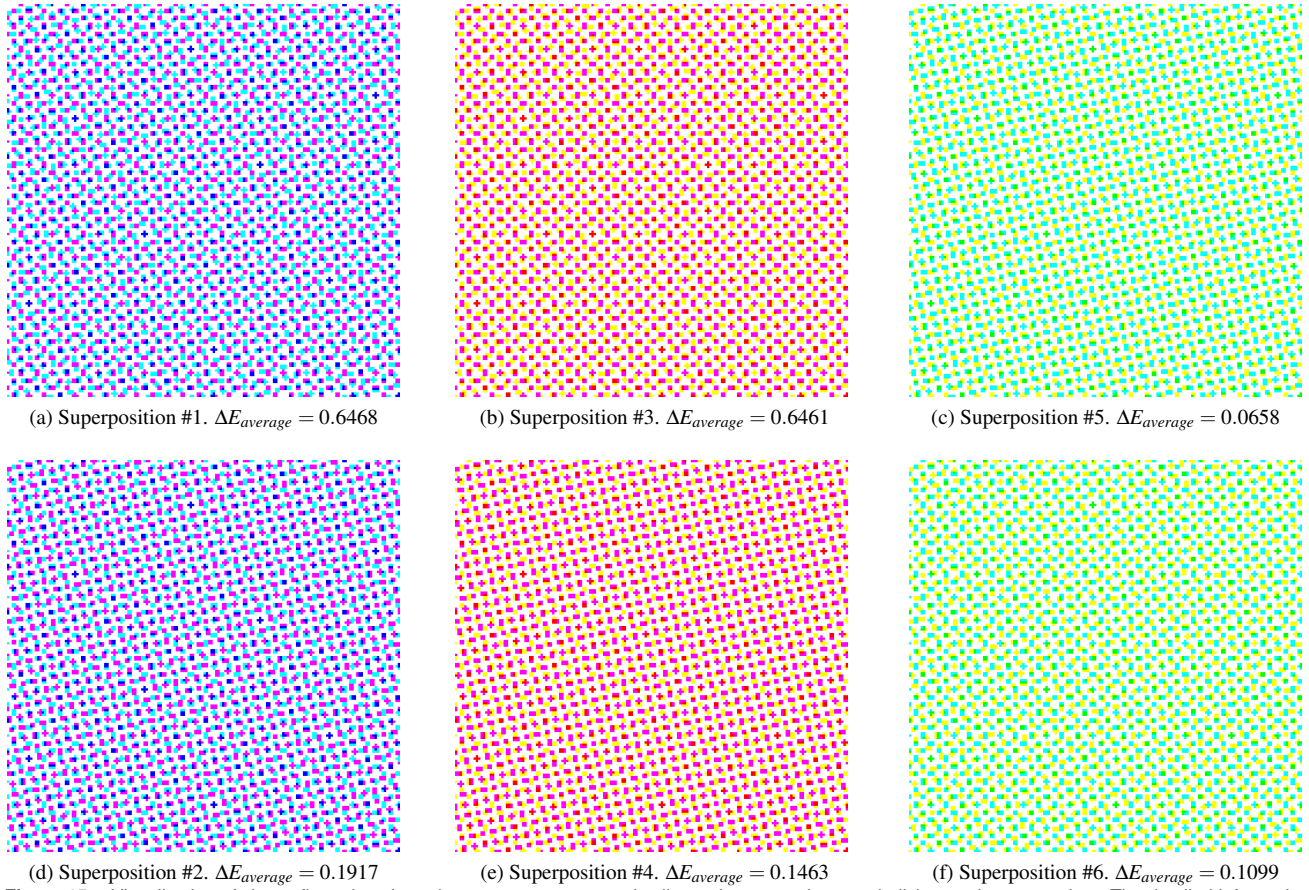


Figure 15. Visualization of six configurations based on cyan, magenta, and yellow colorants and two periodicity matrices N_1 and N_2 . The detailed information is provided in Table 2.

Table 2. Comparison between 6 different configurations for cyan, magenta, and yellow.

Superposition Index	$N_1 = \begin{bmatrix} 9/2 & -1 \\ 1 & 9/2 \end{bmatrix}$	$N_2 = \begin{bmatrix} 10/3 & -10/3 \\ 10/3 & 10/3 \end{bmatrix}$	$\Delta E_{average}$
1	Cyan	Magenta	0.6468
2	Magenta	Cyan	0.1917
3	Yellow	Magenta	0.6461
4	Magenta	Yellow	0.1463
5	Cyan	Yellow	0.0658
6	Yellow	Cyan	0.1099